Renewable and Sustainable Energy Reviews 13 (2009) 1854–1869

Contents lists available at ScienceDirect

Renewable and Sustainable Energy Reviews

journal homepage: www.elsevier.com/locate/rser

Performance of artificially roughened solar air heaters—A review

Vishavjeet Singh Hans [a,*], R.P. Saini [b], J.S. Saini [c]

[a] Department of Mechanical Engineering, PAU, Ludhiana, 141004, Punjab, India
[b] Alternate Hydro Energy Centre, Indian Institute of Technology, Roorkee, 247667, UK, India
[c] Mechanical & Industrial Engineering Department, Indian Institute of Technology, Roorkee, 247667, UK, India

A R T I C L E I N F O

Article history:
Received 7 November 2008
Accepted 20 January 2009

Keywords:
Artificial roughness
Heat transfer
Friction factor
Thermohydraulic performance

A B S T R A C T

The conversion, utilization and recovery of energy invariably involve a heat exchange process, which makes it imperative to design more efficient heat exchanger. The use of artificial roughness in different forms, shapes and sizes is the most common and effective way to improve the performance of a solar air heater. Several studies have been carried out to determine the effect of different roughness element geometries on heat transfer and friction in solar air heaters. This study reviews various roughness element geometries employed in solar air heaters for performance enhancement. Based on the correlations of heat transfer and friction factor developed by various investigators, an attempt has been made to compare the thermohydraulic performance of roughened solar air heaters.

Contents

* Corresponding author. Tel.: +91 99971 10548.
E-mail address: vshandah@iitr.ernet.in (V.S. Hans).

1364-0321/$ – see front matter
doi:10.1016/j.rser.2009.01.030

Nomenclature

A	effective area of collector (m^2)
B	half-length of v-rib element (m)
C	conversion factor to convert high-grade mechanical energy (pumping power) to equivalent thermal energy
d	distance of gap from side wall of duct (m)
D	equivalent diameter of duct (m)
e	roughness height (m)
En	energy flow rate (W)
f	friction coefficient of rough surface
f_s	friction coefficient of smooth surface
g	width of gap (m)
G	global irradiation (W/m^2)
H	height of duct (m)
I	incident radiations (W/m^2)
p	pitch (m)
P	friction (pumping) power (W)
p'	staggering pitch (m)
Q_U	useful gain (W)
S	length of main segment of rib element (m)
S'	length of staggered rib element (m)
W	width of duct (m)
y	distance from wall (m)

Dimensionless symbols

B/S	relative roughness length ratio
d/W	relative gap position
e/d	relative roughness height
e^+	roughness Reynolds number
g/e	relative gap width
l/s	relative grit length
L/e	relative longway length of wire mesh
Nu	Nusselt number for rough surface
Nu_s	Nusselt number for smooth surface
p'/p	relative staggering pitch ratio
p/e	relative roughness pitch
Re	Reynolds number
S'/S	relative staggering ratio
S/e	relative shortway length of wire mesh
St	Stanton number
u^+	dimensionless velocity = $u\sqrt{(\tau_w/\rho)}$
u_t	friction velocity (m/s) = $u_m\sqrt{(f/2)}$
u_m	mean flow velocity (m/s)
y^+	dimensionless distance = $y\,[\sqrt{(\tau_w/\rho)}]/\upsilon$

Greek symbols

α	angle of attack (°)
Φ	chamfer/wedge angle (°)
τ_w	wall shear stress (Pa)
ρ	density of fluid (kg/m^3)
υ	kinematic viscosity of fluid (m^2/s)
η_{th}	thermal efficiency of collector
δ_t	thickness of laminar sub layer (m)
η_c	Carnot efficiency based on mean fluid temperature as source and ambient temperature as sink
η_{eff}	effective efficiency
ε	thermo-hydraulic performance parameter
$\acute{e}$	enhancement factor

1. Introduction

Increase in global demand and consumption of energy, on account of economic development, technological and population growth, has forced the scientific community to think of ways and means to conserve energy in every industrial, commercial and domestic application. The conversion, utilization and recovery of energy invariably involve a heat exchange process, which makes it imperative to improve the thermal performance of heat exchangers [1]. Several viable engineering solutions, particularly with the use of heat transfer enhancement techniques, are available to achieve this objective. Constantinos [2] classified the enhancement techniques as fluid, surface and compound enhancement techniques. Representative examples of each technique are given in Table 1 [3–34].

Heat transfer enhancement techniques have been employed to improve the performance of a solar air heater which is the simplest and most commonly used device in solar energy applications, requiring low grade thermal energy, such as drying of agricultural produce, seasoning of wood, space heating, curing of industrial products. Performance of a solar air heater is adversely affected on account of low thermal capacity of air and absorber to air convective heat transfer coefficient, which needs design considerations, and to the extent possible, compensation. For this purpose surface techniques, which directly involve the heat-exchanger surface, are employed on the underside of absorber plate that comes in contact with air. These techniques improve the

Table 1
Classification of enhancement methods [2].

Category	Technique	References
Surface methods	Roughened surfaces	[3–12]
	Extended surfaces	[13–15]
	Corrugated surfaces	[16–20]
	Perforated surfaces	[21,22]
	Swirl-flow devices	[23–26]
	Surface vibrations	[27]
	Surface rotation	[28,29]
Fluid methods	Fluid vibration	[30]
	Fluid additives	[31]
	Electrostatic fluids	[32]
Compound methods	Vibration/roughened	[30]
	Perforations/corrugations	[33]
	Roughened/rotation	[34]

thermal performance either by increasing the heat-transfer area with the use of corrugated/finned absorber surfaces or by enhancing the absorber to air convective heat transfer coefficient with the use of roughened absorber surfaces. The roughness, on the absorber plate can be provided by several methods such as sand blasting, machining, casting, forming, welding ribs and or fixing thin circular wires. The use of artificial roughness in different forms and shapes is the most effective and economic way of improving the performance of a solar air heater. Numbers of experimental investigations involving roughness elements of different shapes, sizes and orientations with respect to flow direction have been carried out in order to obtain an optimum arrangement of roughness element geometry. Varun et al. [35] carried out a review of roughness geometry in solar air heaters. They discussed different roughness geometries used in solar air heaters and explained the concept of artificial roughness, effects of various roughness parameters on the flow pattern and also briefly discussed the roughness geometries used in heat exchangers other than solar air heaters. Mittal et al. [36] compared the effective efficiency of solar air heaters having six different types of roughness elements on the absorber plate and reported that solar air heaters roughened with inclined ribs and wire mesh perform better in the upper and lower range of parameters considered respectively.

However, since then a number of new roughness element geometries have been reported in literature and there is a need to categorize and compare the performance of these geometries. The objective of the present work is to review roughness element geometries used in solar air heaters for performance enhancement. In this study, 23 roughness geometries have been considered and technical information so obtained has been used to determine the best performing roughness element geometry from thermohydraulic point of view.

2. Concept of artificial roughness

As the air flows through the duct of a solar air heater, a laminar sublayer is formed over the absorber surface that impedes the heat transfer to the flowing air, thereby, adversely affecting the thermal performance of the solar air heater. The primary mechanisms for thinning the boundary layer are increased free stream velocity and turbulent mixing. Artificial roughness, provided on the underside of the absorber plate, creates local wall turbulence. Secondary recirculation flows further enhance the convective heat transfer. Flows from the core to the surface reduce the thickness of boundary layer and secondary flows from the surface to the core flow promote mixing. Energy for creating turbulence has to come from a blower and excessive turbulence results in greater power requirements for the blower. So, it becomes necessary that turbulence must be created in laminar sub layer region where heat transfer takes place. In order to select height of the artificial roughness element, it becomes imperative to know the thickness of the laminar sublayer which is expressed by the following equation [37]

$$\delta_t = 5 \times \frac{\nu}{u_t} \quad (1)$$

Fluid flow and heat transfer characteristics of roughened surface

Early studies, beginning with that of Nikuradse [38], attempted to develop velocity and temperature distribution for roughened surfaces.

2.1.1. For smooth surface

$$u^+ = y^+ \text{ for laminar sublayer}, y^+ \le 5 \quad (2)$$

$$u^+ = 5\ln y^+ + 3.5 \text{ for buffer layer}, 5 \le y^+ \le 30 \quad (3)$$

$$u^+ = 2.5\ln y^+ + 5.5 \text{ for turbulent layer}, y^+ > 30 \quad (4)$$

2.1.2. For roughened surface

For roughened surfaces, a parameter called roughness Reynolds number (e^+) has been defined for flow analysis and is expressed as

$$e^+ = \frac{e}{D}\sqrt{\frac{f}{2}}Re \quad (5)$$

$R(e^+)$ known as momentum transfer function and can be written as:

$$R(e^+) = \sqrt{\frac{2}{f}} + 2.5\ln\left(\frac{2e}{D}\right) + 3.75 \quad (6)$$

A similar relation for heat transfer in terms of a heat transfer function $G(e^+)$ has been developed by Dippery and Sabersky [39] for roughened circular pipes and is expressed as:

$$G(e^+) = \left[\frac{f}{2St} - 1\right]\sqrt{\frac{f}{2}} + R(e^+) \quad (7)$$

The different types of roughness elements and the parameters that characterize the roughness element geometry and influence the performance are given in Table 2.

3. Effect of rib parameters on flow pattern

3.1. Effect of a rib

Artificial roughness provided on the underside of the absorber plate creates two flow separation regions, one on each side of the

Table 2
Rib geometries and important parameters.

S. no.	Rib geometry	Parameter
1.	Transverse ribs	(e/d), (p/e)
2.	Continuous angled ribs	(e/d), (p/e), α
3.	Angled ribs with gaps	(e/d), (p/e), α, g/P, d/W
4.	V-shaped ribs	(e/d), (p/e), α
5.	V-shaped staggered discrete ribs	(e/d), (p/e), α, B/S, p'/p, S'/S
6.	Transverse-chamfered ribs	(e/d), (p/e), Φ
7.	Grooved-ribbed arrangement	(e/d), (p/e), g/P
8.	Arc shaped ribs	(e/d), (p/e), α
9.	W-shaped discrete ribs	(e/d), (p/e), α
10.	Wire mesh	((e/d), (p/e), L/e, S/e

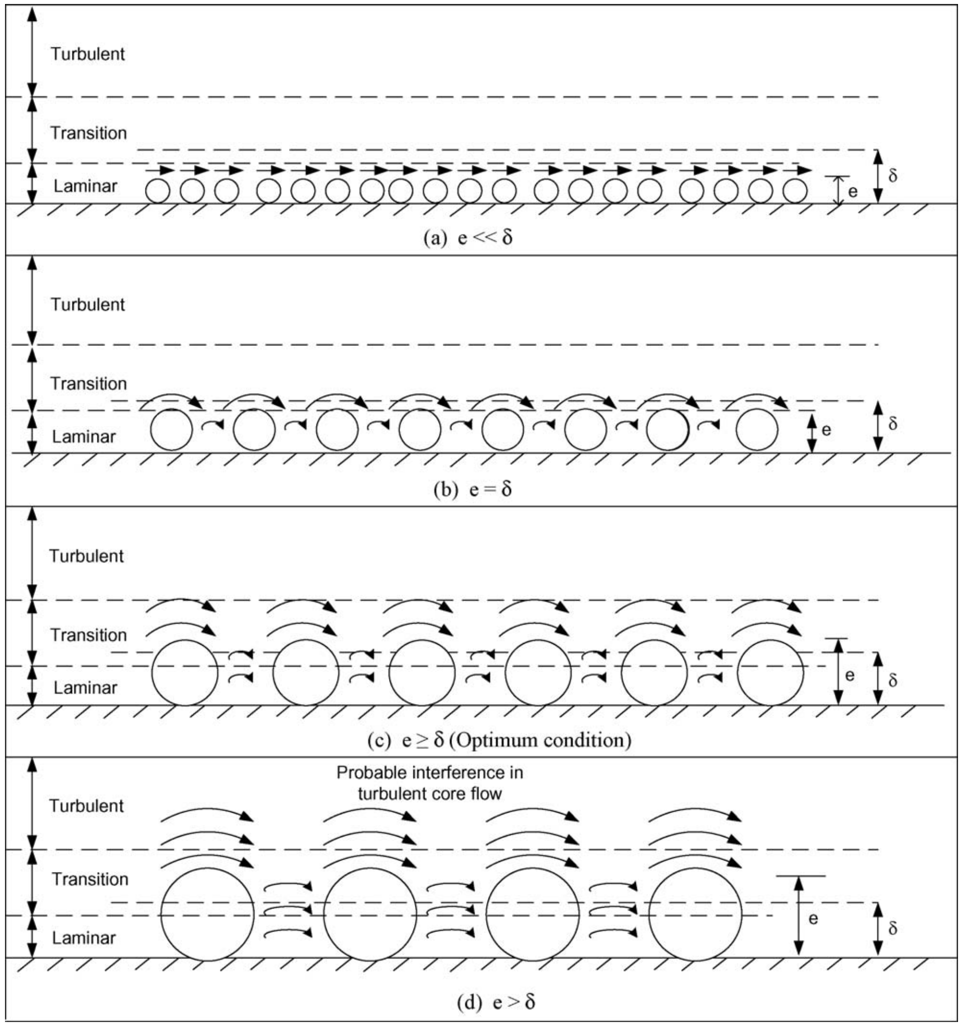


Fig. 1. Effect of rib height on laminar sub layer [40].

rib, and vortices so generated are responsible for turbulence, which promotes heat transfer accompanied by friction losses. Fig. 1 shows the effect of rib height on laminar sub layer [40].

3.2. Effect of rib height and pitch

Figs. 2 and 3 show the flow patterns downstream of a rib with variation in rib height and pitch [41]. The flow separation occurs downstream of a rib and reattachment does not occur if relative roughness pitch (p/e) is less than 8. Maximum heat transfer occurs in the vicinity of reattachment point. Similarly, by decreasing the relative roughness pitch (p/e) for fixed relative roughness height (e/D) or by increasing relative roughness height (p/e) for fixed relative roughness pitch (e/D), heat transfer is enhanced. An upper limit of 10 has been imposed on relative roughness pitch (p/e) beyond which there is a decrease in heat transfer enhancement.

3.3. Effect of inclination of rib

The angling of the rib with respect to flow creates counter-rotating secondary flow along the span that causes span wise variation of heat transfer coefficient. The vortices move along the rib to subsequently join the main stream i.e. the fluid enters at the leading end of the rib and comes out near the trailing end as shown in Fig. 4. The moving vortices bring the cooler channel fluid in contact with leading end, raising heat transfer rate while the trailing end heat transfer is relatively low. This results in strong span wise variation of heat transfer [42].

3.4. Effect of width and position of gap in continuous inclined rib

With the introduction of a gap in a rib, secondary flow along the rib joins the main flow to accelerate it, which in turn, energizes the retarded boundary layer flow along the surface resulting in enhancement of heat transfer. Position of gap with respect to leading and trailing edge has a considerable effect on heat transfer enhancement. Position of the gap near the trailing edge, results in more contribution of secondary flow in energizing the main flow through the gap and recirculation loop in the remaining part of the rib, thereby, increasing the heat transfer rate as shown in Fig. 5 [43].

3.5. Effect of v-shaping of rib

Shaping of a long, angled rib into v-shape helps in the formation of two leading ends (where heat transfer rate is high) and a single trailing end (where heat transfer is low) resulting in much large area of heat transfer. V-shaped ribs form two secondary flow cells as compared to one in case of a straight angled rib resulting in higher overall heat transfer coefficient in case of v-shaped rib as shown in Fig. 6. V-shaped rib with apex facing downstream has a

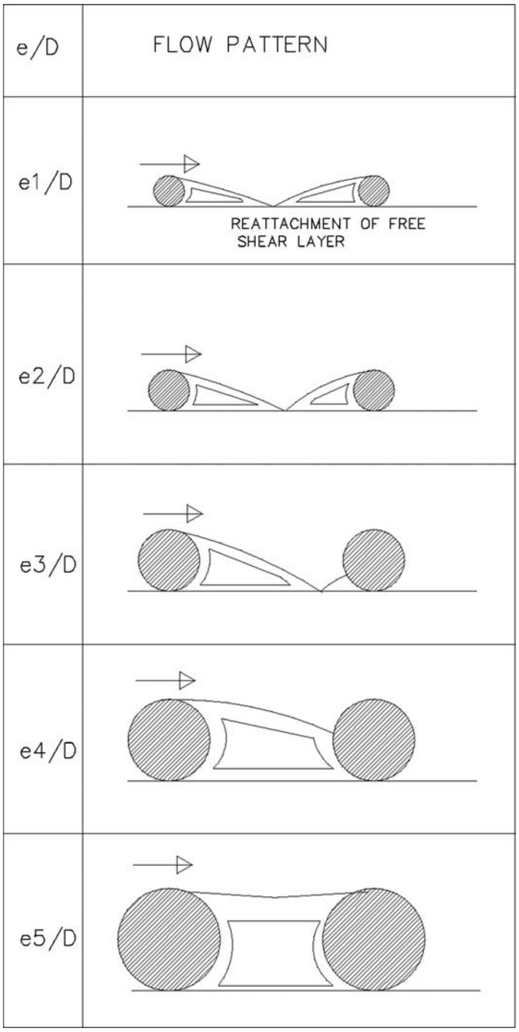


Fig. 2. Effect of rib roughness height on flow pattern ($e_5 > e_4 > e_3 > e_2 > e_1$, p = constant) [41].

higher heat transfer as compared to that of with apex facing upstream [42].

3.6. Effect of discretizing of v-shaped ribs

The v-shaped ribs along with staggered rib pieces in between further increase the number and area of heat transfer regions. Additional rib parameters related to the size and positioning of rib pieces (length ratio, B/S, segment ratio, S'/S and staggering ratio, P'/P) with respect to main rib produce complex interaction of secondary flow [44].

3.7. Effect of rib cross-section

Rib cross-section affects the size of separated region and level of disturbance in the flow. The friction factor is less for circular cross-section ribs in comparison to that of rectangular or square cross-section ribs on account of reduction in the size of separated region. This results in decrease in inertial losses and increase in skin friction, thereby, decreasing the friction factor. As the size of separated region diminishes, level of disturbance in flow also decreases which affects the heat transfer adversely. Another possible factor contributing to the Nusselt number decrease is the reduction in heat transfer surface area associated with circular cross-section ribs [45].

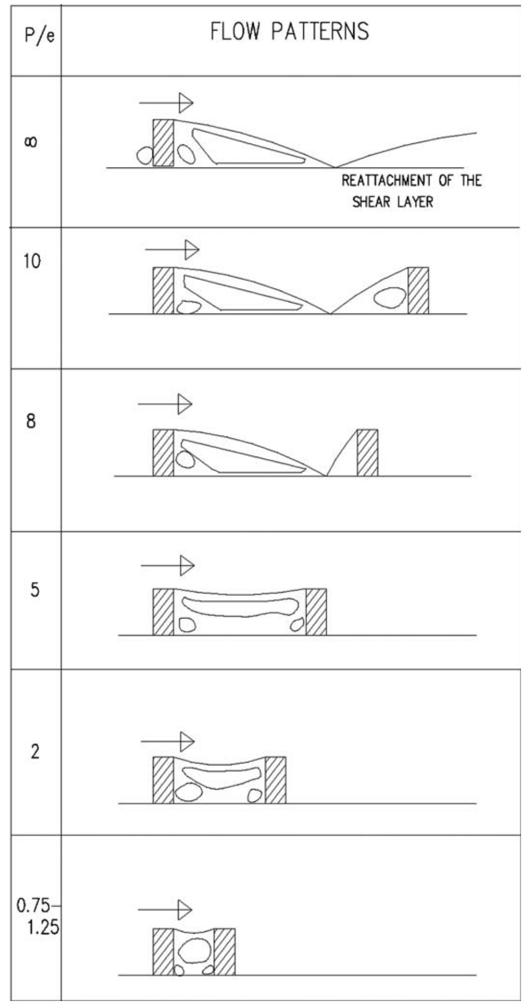


Fig. 3. Flow pattern of rib as a function of relative roughness pitch [41].

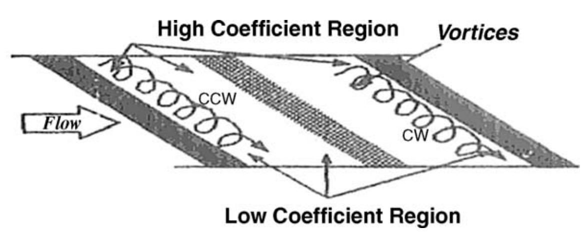


Fig. 4. Effect of inclination of rib [42].

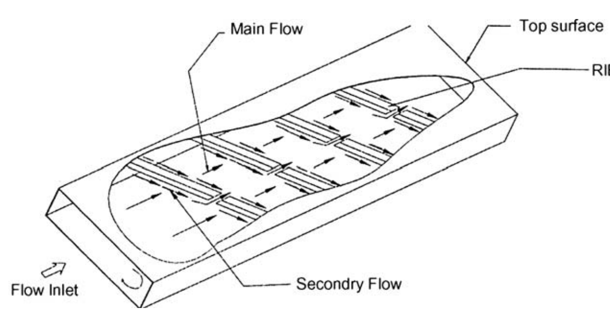


Fig. 5. Effect of width and position of gap in broken inclined rib [43].

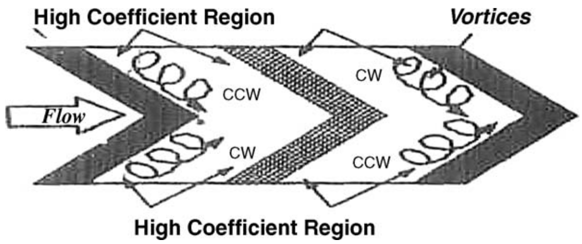


Fig. 6. Effect of v-shaping of rib [42].

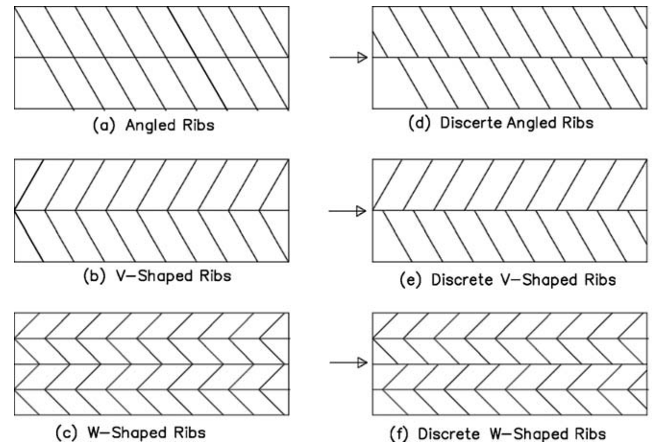


Fig. 7. Top view of rib configurations used by Wright et al. [52].

4. Thermo-hydraulic considerations

Performance of a solar air heater depends upon the heat transfer between absorber plate and air flowing through it. Heat transfer rate for turbulent flow is higher than that of laminar flow and different roughness geometries are used to introduce turbulence for better fluid mixing. However, any roughness geometry that enhances heat transfer is most likely to increase pressure drop also. To account for the pressure drop in the performance of roughness geometry, following criteria that combine thermal and hydraulic performance are generally used.

4.1. Thermo-hydraulic performance parameter

Lewis [46] used the following parameter (ε) in terms of Stanton number and friction factor ratios for roughened and smooth surfaces, all operated at the same channel Reynolds number (Re)s.

$$\varepsilon = \frac{(\mathrm{St}/\mathrm{Sts})^3}{(f/fs)} \tag{8}$$

4.2. Energy flow considerations

Altfeld et al. [47] proposed a method based on second law of thermodynamics and the increase of energy of air while passing through the collector can be written as

$$\mathrm{En} = GA\,\eta_{\mathrm{th}}\eta_{\mathrm{c}} - P(1-\eta_{\mathrm{c}}) \tag{9}$$

4.3. Effective efficiency

Cortes and Piacentini [48] defined effective efficiency on the basis of net thermal gain which is obtained by subtracting the equivalent thermal energy that will be required to produce friction power from collector gain and is written as

$$\eta_{\mathrm{e}} = \frac{(Qu - P/C)}{A.I.} \tag{10}$$

5. Roughness geometries used in solar air heaters

An effort that began 147 years ago, when the first attempt to enhance heat transfer coefficients in condensing steam was reported in the classical study by JP Joule [49], continues to be a major research and development activity [50,51]. The use of artificial roughness in solar air heaters owes its origin to several investigations carried out in connection with the enhancement of heat transfer in nuclear reactors, cooling of turbine blades and electronic equipment. Important roughness geometries reported in literature are shown in Figs. 7–9 [52–54].

Kays [55] suggested the use of small diameter circular wires to artificially roughen the heat transferring surface of a heat exchanger to enhance heat transfer and recommended that in order to make the use of artificial roughness more effective, the height of roughness element should be kept small, primarily in the sublayer region, so that the increases in the friction will not be disproportionate to the increase in heat transfer.

The different types of roughness element geometries investigated by researchers are discussed as:

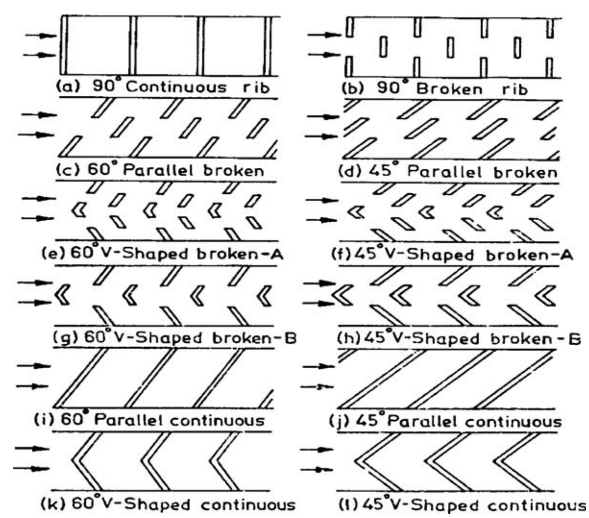


Fig. 8. Top view of rib configurations used by Han et al. [53].

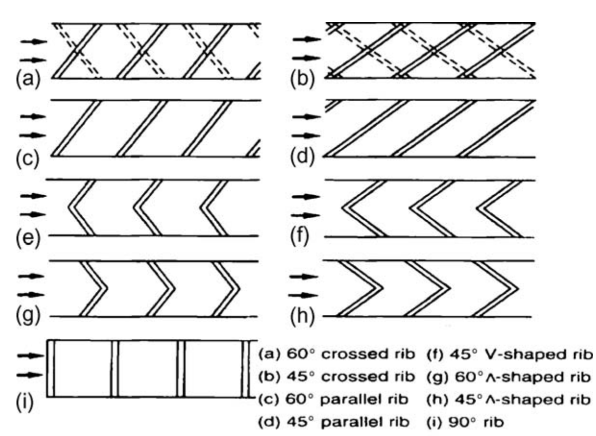


Fig. 9. Top view of rib configurations used by Han and Zhang [54].

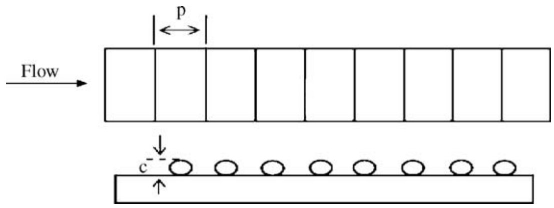


Fig. 10. Transverse continuous ribs [40].

5.1. Transverse continuous ribs

5.1.1. Ribs of circular cross-section

Prasad and Mullick [56] studied the effect of protruding wires on friction factor, heat transfer coefficient and plate efficiency factor of a solar air heater used for drying of agricultural products. High mass flow rates were used to have turbulent flow in the ducts and protruding wires of 1 mm diameter tripped the laminar sublayer. They compared the Nusselt number, friction factor and plate efficiency factor of roughened corrugated and plane absorber plates with that of plane corrugated and smooth absorber plates. The protruding wires enhanced the heat transfer coefficient for the roughened air heaters and plate efficiency factor improved from 0.63 to 0.72 resulting in 14% improvement in the performance.

Prasad and Saini [40,41] studied the effect of roughness and flow parameters such as relative roughness height (e/D) and relative roughness pitch (p/e) on heat transfer and friction factor. The type and orientation of roughness geometry used have been shown in Fig. 10. They developed expressions for the heat transfer and friction factor for a fully turbulent flow. It was observed that maximum heat transfer occurred in the vicinity of reattachment points and reattachment of free shear layer does not occur if relative roughness pitch (p/e) is less than about 8 to 10. Optimal thermohydraulic performance is achieved for roughness height slightly higher than the transition sublayer thickness. For relative roughness height (e/D) value of 0.033 and relative roughness pitch (p/e) value of 10, maximum enhancement in Nusselt number and friction factor was reported to be 2.38 and 4.25 times respectively over smooth duct.

With the previous investigations [40,41,56] carried out for fully rough flow conditions ($e^+ > 70$), Gupta et al. [57] carried out an experimental investigation for transitionally rough flow region ($e^+ < 50$) in which most of the solar air heaters operate efficiently and developed correlations for friction factor and Nusselt number over a wide range of roughness element parameters. They studied heat transfer and friction characteristics of a rectangular duct roughened with transverse wires, with relative roughness height (e/D) varying from 0.018 to 0.052, aspect ratio (W/H) range of 6.8–11.5 and Reynolds number (Re) range of 3000–18,000 for a fixed value of relative roughness pitch (p/e) of 10. It was observed that for fully rough flow region, Stanton number decreased monotonously with increase in Reynolds number (Re) for a given roughness configuration. In transitionally rough flow region, Stanton number increased with increase in Reynolds number (Re) and attained a point of maxima for Reynolds number (Re) value of about 12,000. The point of maxima shifted towards lower values of Reynolds number (Re) as the value of relative roughness height (e/D) increased.

Verma and Prasad [58] carried out an outdoor experimental investigation for thermohydraulic optimization of the roughness and flow parameters for Reynolds number (Re) range of 5000–20,000, relative roughness pitch (p/e) range of 10–40 and relative roughness height (e/D) range of 0.01–0.03. The optimal value of roughness Reynolds number (e^+) was found to be 24 and corresponding to this value, optimal thermohydraulic performance was reported to be 71%. Heat transfer enhancement factor was found to vary between 1.25 and 2.08 for the range of parameters investigated. Correlations for heat transfer and friction factor were developed.

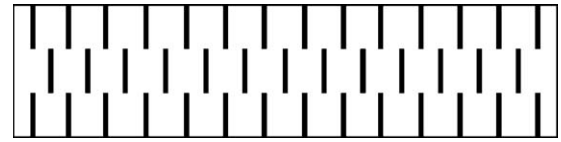


Fig. 11. Transverse broken ribs [60].

5.1.2. Ribs of rectangular cross-section

Karwa [59] experimentally investigated the effect of repeated rectangular cross-section ribs on heat transfer and friction factor for duct aspect ratio (W/H) range of 7.19–7.75, relative roughness pitch (p/e) value of 10, relative roughness height (e/D) range of 0.0467–0.050, Reynolds number (Re) range of 2800–15,000. It was explained that vortices originating from the roughness elements beyond the laminar sublayer were responsible for heat removal as well as increase in friction factor. The enhancement in the Stanton number was reported to be 65–90% while friction factor was found to be 2.68–2.94 times over smooth duct.

5.2. Transverse broken ribs with circular cross-section

Sahu and Bhagoria [60] investigated the effect of 90° broken ribs on thermal performance of a solar air heater for fixed roughness height (e) value of 1.5 mm, duct aspect ratio (W/H) value of 8, pitch (p) in the range of 10–30 mm and Reynolds number (Re) range of 3000–12,000. Roughened absorber plate increased the heat transfer coefficient by 1.25 to 1.4 times as compared to smooth one under similar operating conditions. Corresponding to roughness pitch (p) value of 20 mm, maximum value of Nusselt number was obtained that decreased on the either side of this roughness pitch (p) value. Based on the experimental investigation, the thermal efficiency of roughened solar air heater was found to be in the range of 51–83.5% depending upon the flow conditions. The geometry investigated has been shown in Fig. 11.

5.3. Inclined continuous ribs

5.3.1. Ribs of circular cross-section

Gupta et al. [61] experimentally investigated the effect of relative roughness height (e/d), inclination of rib with respect to flow direction and Reynolds number (Re) on the thermohydraulic performance of a roughened solar air heater for transitionally rough flow region ($5 < e^+ < 70$). The roughness geometry investigated has been shown in Fig. 12. It was reported that with increase in relative roughness height (e/d), the value of Reynolds number (Re) decreased for which effective efficiency was maximum. The effective efficiency also increased with increase in insolation. For a roughened solar air heater, maximum enhancement in heat transfer and friction factor was reported to be of the order 1.8 and 2.7 times respectively corresponding to angle of inclination values of 60° and 70°, respectively. Best

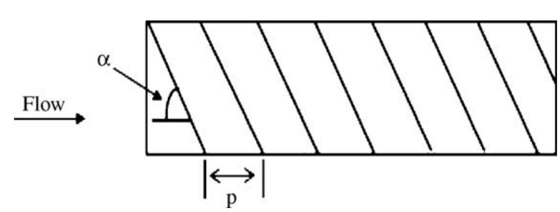


Fig. 12. Inclined continuous ribs [61].

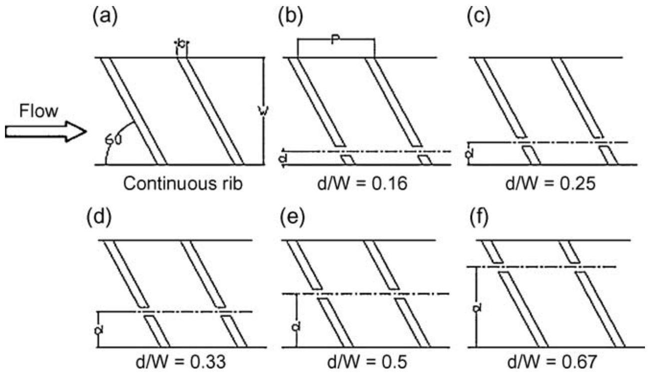


Fig. 13. Inclined ribs with gap [43].

thermohydraulic performance was reported for relative roughness height (e/D) value of 0.023 and Reynolds number (Re) value of 14,000.

5.3.2. Ribs of rectangular cross-section

Karwa [59] experimentally investigated the effect of repeated, 60° inclined rectangular cross-section ribs on heat transfer and friction factor for aspect ratio (W/H) range of 7.19–7.75, relative roughness pitch (p/e) value of 10, relative roughness height (e/d) range of 0.0467–0.050 and Reynolds number (Re) range of 2800–15,000. The enhancement in the Stanton number was reported to be 22–32% and increase in friction factor was of the order of 1.12–1.16 times over transverse ribs.

5.3.3. Inclined broken ribs

Aharwal et al. [43] experimentally studied the effect of width and position of gap in inclined split-ribs having square cross-section on heat transfer and friction characteristics of a rectangular duct. The duct had an aspect ratio (W/H) of 5.84, relative roughness pitch (p/e) of 10, relative roughness height (e/D) of 0.0377, angle of attack (α) of 60°, relative gap width (g/e) range of 0.5–2 and relative gap position (d/W) varied from 0.1667 to 0.667 for Reynolds number (Re) range of 3000–18,000. For the split-rib and continuous rib roughened ducts, the enhancement in heat transfer was reported to be in the range of 1.71–2.59 and 1.48–2.26 times respectively over smooth duct under similar operating conditions. The maximum values of heat transfer, friction factor ratio (f/f_s) and thermohydraulic parameter so obtained were corresponding to relative gap width (g/e) value of 1.0 and relative gap position (d/W) value of 0.25 for the range of parameters investigated. Particle Image Velocimetry (PIV) system was used to visualise the effects of angle of inclination of ribs on the flow behavior. Based on experimental results, correlations for Nusselt number and friction factor were developed. The geometry investigated has been shown in Fig. 13.

5.4. Expanded mesh metal

Saini and Saini [62] carried out an experimental investigation to study the effect of wire mesh roughened absorber plate on heat transfer augmentation and friction characteristics of solar air heater as shown in Fig. 14. The investigation considered relative longway length of mesh (L/e) in range of 25–71.87, relative shortway length of mesh (S/e) in range of 15.62–46.87, relative roughness height (e/D) in range of 0.12–0.039 and Reynolds number (Re) in range of 1900–13,000. It was reported that the maximum heat transfer of order 4 times over the smooth duct was obtained corresponding to angle of attack of 61.9°, relative longway length of mesh (L/e) value of 46.87 and relative shortway length of mesh (S/e) value of 25. Maximum value of friction factor was reported for angle of attack of 72°, relative longway length of mesh (L/e) value of 71.87 and relative shortway length of mesh (S/e) value of 15. Correlations for Nusselt number and friction factor were developed.

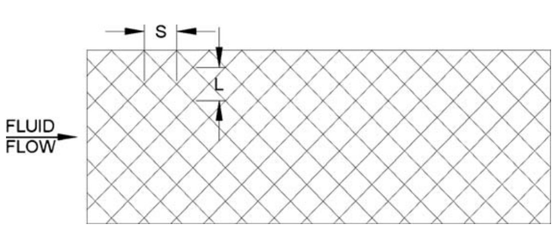


Fig. 14. Wire mesh roughness [62].

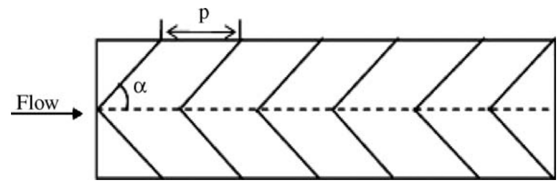


Fig. 15. V-shape ribs [63].

5.5. V-shaped ribs

5.5.1. V-shaped continuous ribs

Momin et al. [63] experimentally investigated the effect of geometrical parameters of v-shaped ribs, shown in Fig. 15, on heat transfer and fluid flow characteristics of rectangular duct of a solar air heater. The investigation covered a Reynolds number (Re) range of 2500–18,000, relative roughness height (e/D) range of 0.02–0.034 and angle of attack of flow (α) range of 30–90° for a fixed relative roughness pitch (p/e) value of 10. Rate of increase of Nusselt number was observed to be lower than the rate of increase of friction factor with an increase in Reynolds number (Re). The maximum enhancement of Nusselt number and friction factor as result of providing artificial roughness had been found to be 2.30 and 2.83 times respectively over the smooth duct for an angle of attack (α) of 60°. It was reported that for relative roughness height (e/D) value of 0.034 and angle of attack (α) of 60°, v-shaped ribs enhanced the value of Nusselt number by 1.14 and 2.30 times over inclined ribs and smooth absorber plate respectively. Correlations for Nusselt number and friction factor were developed.

5.5.2. V-shaped staggered discrete ribs

Muluwork et al. [44] compared the thermal performance of staggered discrete v-apex up and down ribs with corresponding transverse staggered discrete ribs shown in Fig. 16. They studied the effect of relative roughness length ratio (B/S), relative roughness segment ratio (S'/S), relative roughness staggering ratio (p'/p) and angle of attack (α) on the heat transfer and friction factor. It was observed that the Nusselt number increased with the increase in relative roughness length ratio (B/S). Nusselt number for v-down discrete ribs was found to be higher than

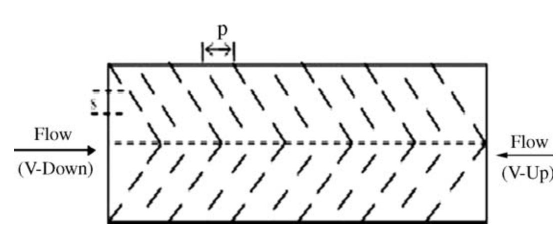


Fig. 16. Discrete v-shape ribs [44].

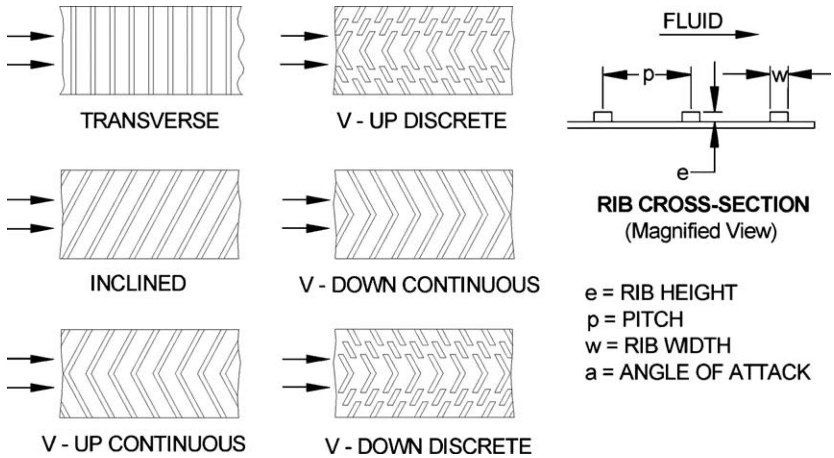


Fig. 17. Roughness geometries used by Karwa [59].

the corresponding v-up and transverse discrete roughened surfaces. Nusselt number increased with increase in relative roughness staggering ratio (p'/p) and attained a maximum value for relative roughness staggering ratio (p'/p) value of 0.6. Heat transfer and friction factor attained maximum values for angle of attack (α) 60° and 70°, respectively. Correlations for Nusselt number and friction factor were developed.

Karwa [59] carried out a comparative experimental study of augmented heat transfer and friction in a rectangular duct with rectangular cross-section ribs arranged in v-continuous and v-discrete pattern for duct aspect ratio (W/H) range of 7.19–7.75, relative roughness pitch (p/e) value 10, relative roughness height (e/D) range of 0.0467–0.050 and Reynolds number (Re) range of 2800–15,000. The enhancement in the Stanton number over the smooth duct was reported to be in range of 102–137%, 110–147%, 93–134% and 102–142% for transverse, inclined, v-up continuous, v-down continuous, v-up discrete and v-down discrete rib arrangement, respectively. The friction factor ratios corresponding to these arrangements were found as 3.02–3.42, 3.40–3.92, 3.32–3.65, 2.35–2.47 and 2.46–2.58, respectively. The performance of v-down ribs was observed to be better than that of v-up ribs, which was in confirmation with the findings of Muluwork et al. [44]. The rib configurations investigated in the study have been shown in Fig. 17.

Karwa et al. [64] experimentally studied the heat transfer and friction in a high aspect ratio (W/H) rectangular duct with repeated rectangular cross-section ribs on one broad wall in v-discrete and discontinuous patterns at angles of inclination of 45° and 60°, relative roughness pitch (p/e) value of 10.63, relative roughness length (B/S) values 3 and 6 with Reynolds number (Re) varied from 2850 to 15500. It was observed that corresponding to relative roughness length (B/S) value of 6; the highest and the lowest values of Stanton number ratio (St/St_s) were obtained for 60° v-down discrete and 60° v-up discontinuous ribs, respectively. Friction factor ratio (f/f_s) values were found to be maximum and minimum for the 60° v-down discrete and 45° v-up discrete ribs corresponding to relative roughness length (B/S) value of 3. Stanton number and friction factor values were reported to be higher for v-down pattern in comparison with v-up pattern and 60° v-shaped ribs performed better than the 45° v-shaped ribs. Rib pattern had a strong effect on the Stanton number and friction factor with discrete ribs performing better than other rib configurations from thermohydraulic performance point of view. The various v-rib configurations investigated have been shown in Fig. 18.

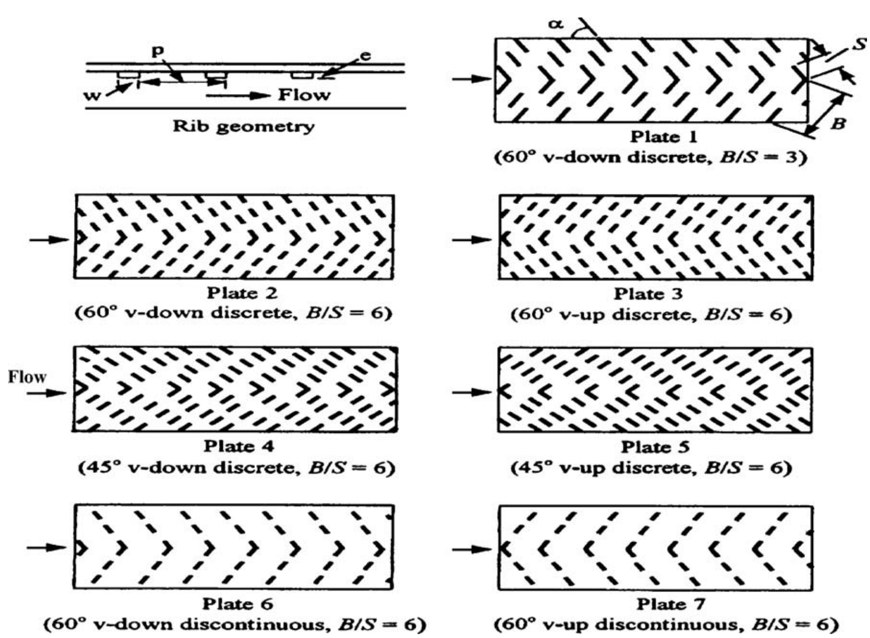


Fig. 18. V-shape ribs of different configurations [64].

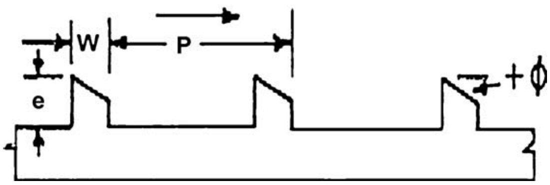


Fig. 19. Chamfered ribs [65].

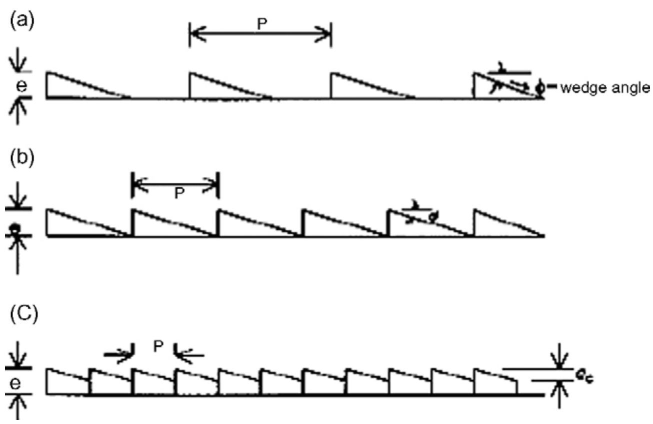


Fig. 20. Wedge shape ribs [66].

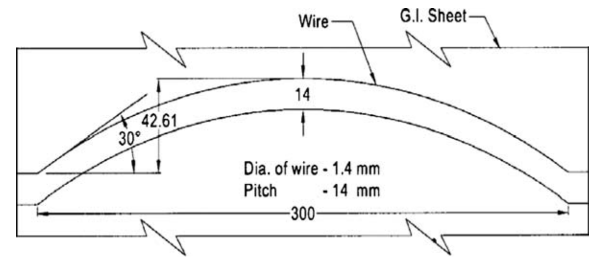


Fig. 21. Arc shape ribs [67].

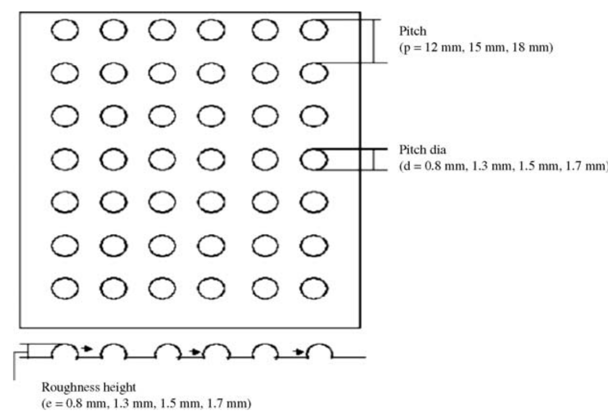


Fig. 22. Dimple shape ribs [68].

5.6. Chamfered ribs

Karwa et al. [65] performed an experimental investigation of heat transfer and fiction for rectangular ducts, having aspect ratio (W/H) in the range of 4.8–12, and roughened with repeated integral chamfered ribs, as shown in Fig. 19. The roughness parameters considered for the investigation were Reynolds number (Re) range of 3000–20,000, relative roughness height (e/D) range of 0.014–0.0328, relative roughness pitch (p/e) range of 4.5–8.5 and chamfer angle (Φ) varying from -15° to 18°. Stanton number and friction factor increased with increase in chamfer angle and attained maximum value corresponding to chamfer angle (Φ) value of 15°. It was reported that Stanton number decreased while friction factor increased with increase in aspect ratio (W/H). As compared to smooth duct, the presence of chamfered ribs on the wall of duct yielded up to about two-fold and three-fold increase in the Stanton number and the friction factor respectively in the range of parameters investigated. Heat transfer and friction factor correlations were developed.

5.7. Wedge shaped ribs

Bhagoria et al. [66] experimentally studied heat transfer and flow characteristics in a solar air heater having absorber plate roughened with wedge shaped transverse integral ribs as shown in Fig. 20. The investigation encompassed the Reynolds number (Re) range of 3000–18,000, relative roughness height (e/D) range of 0.015–0.033 and rib wedge angle (Φ) range of 8–12°. It was reported that Nusselt number and friction factor increased by 2.4 and 5.3 times over smooth duct in the range of parameters investigated. Statistical correlations for Nusselt number and friction factor were developed.

5.8. Arc shaped ribs

Saini and Saini [67] studied the effect of arc shaped ribs on the heat transfer coefficient and friction factor of rectangular ducts with Reynolds number (Re), relative roughness height (e/D) and relative arc angle (α) varying from 2000 to 17,000, 0.0213 to 0.0422 and 0.3333 to 0.6666, respectively. It was reported that relative arc angle (α) had an opposite effect on heat transfer enhancement and friction factor. With decrease in relative arc angle (α) value, Nusselt number value increased while friction factor value decreased. Enhancement of Nusselt number and friction factor was reported to be of order 3.6 and 1.75 times respectively over smooth duct for relative arc angle (α) value of 0.3333 and relative roughness height (e/D) value of 0.0422. Based on the experimental results, correlations for Nusselt number and friction factor were developed. The geometry investigated has been shown in Fig. 21.

5.9. Dimpled surfaces

Saini and Verma [68] studied the effect of roughness and operating parameters on heat transfer and friction factor in a roughened duct provided with dimple-shape roughness geometry for the range of Reynolds number (Re) from 2000 to 12,000, relative roughness height (e/D) from 0.018 to 0.037 and relative pitch (p/e) from 8 to 12. For the range of parameters investigated, Nusselt number was found to be maximum corresponding to relative roughness height (e/D) value of 0.0379 and relative roughness pitch (p/e) value of 10. For fixed value of relative roughness pitch (p/e) of 10, friction factor attained the maximum and minimum values corresponding to relative roughness height (e/d) values of 0.0289 and 0.0189, respectively. Correlations for Nusselt number and friction factor have been developed. The geometry investigated has been shown in Fig. 22.

5.10. Metal grit ribs

Karmare and Tikekar [69] experimentally investigated heat transfer and friction characteristics of a rectangular duct having absorber plate roughened with a defined grid of metal ribs of circular cross-section and the roughness geometry investigated

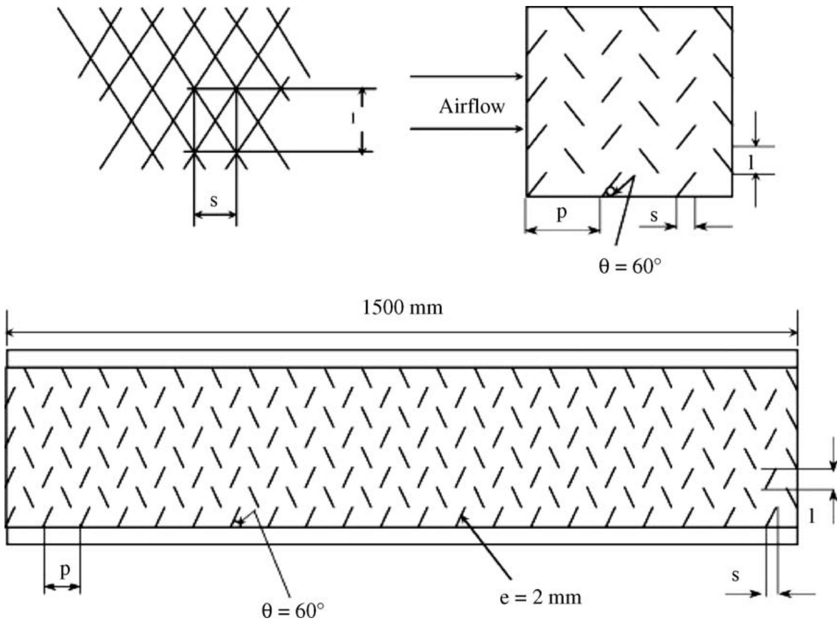


Fig. 23. Metal grit roughness [69].

has been shown in Fig. 23. The investigation considered relative roughness height (e/D) range of 0.035–0.044, relative roughness pitch (p/e) range of 12.5–36, relative grit length (l/s) range of 1–1.72 and Reynolds number (Re) range of 4000–17,000. Enhancement in Nusselt number was found to be 187% and the friction factor increased by 213% and optimum performance was observed for relative grit length (l/s) value of 1.72, relative roughness height (e/D) value of 0.044 and relative roughness pitch (p/e) value of 17.5 for the range of parameters studied. Based on the experimental results, correlations for Nusselt number and friction factor were developed.

5.11. Discrete w-shaped ribs

Kumar et al. [70] carried out an experimental investigation to determine the heat transfer distributions in solar air heater having its absorber plate roughened with discrete w-shaped ribs. The experiment encompassed Reynolds number (Re) range from 3000 to 15,000, rib height (e) values of 0.75 mm and 1 mm, relative roughness height (e/D) 0.0168 and 0.0225 and relative roughness pitch (p/e) of 10 and angle of attack (α) 45°. Thermal performance of roughened solar air collector was compared with that of smooth one under similar flow conditions and it was reported that thermal performance of the roughened channel was 1.2–1.8 times the smooth channel for range of parameters investigated. Discretization was found to have significant effect on heat transfer enhancement. The geometry investigated has been shown in Fig. 24.

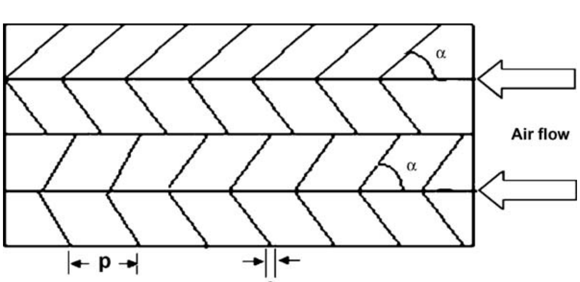


Fig. 24. Discrete w-shape roughness [70].

5.12. Combination of different roughness elements

5.12.1. Rib-groove 1

Jaurker et al. [71] experimentally investigated heat transfer and friction characteristics of rib-groove roughened rectangular duct as shown in Fig. 25. The effect of relative roughness pitch (p/e), relative roughness height (e/D) and relative groove position (g/P) on the heat transfer coefficient and friction factor had been studied. The presence of rib-grooved artificial roughness yielded Nusselt number and friction factor up to 2.7 and 3.6 times respectively in comparison to smooth absorber plate. The maximum heat transfer occurred for a relative roughness pitch (p/e) of about 6 and relative groove (g/P) value of 0.4. Correlations for Nusselt number and friction factor were developed.

5.12.2. Rib-groove 2

Layek et al. [72] carried out an experimental investigation to study heat transfer and friction for repeated transverse compound rib-groove arrangement on absorber plate of a solar air heater. Four relative rib-groove positions (g/P) values of 0.3, 0.4, 0.5 and 0.6 were investigated for fixed relative roughness height (e/D) and relative roughness pitch (p/e) values of 0.03 and 10 respectively. It was found that corresponding to relative roughness pitch (p/e)

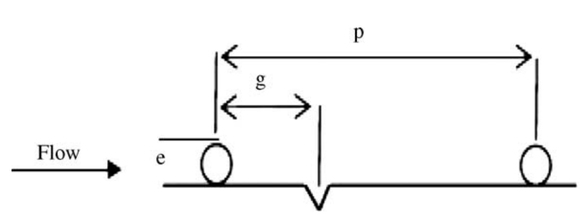


Fig. 25. Combination of transverse and groove roughness [71].

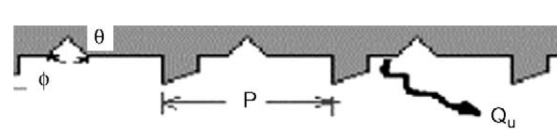


Fig. 26. Combination of chamfered and groove roughness [72].

Table 3
Correlations developed for heat transfer and friction factor for different roughness geometries used in solar air heaters.

Author	Roughness geometry	Parameters	Correlations	
			Heat transfer	Friction factor
Prasad and Saini [40]	Small diameter transverse wires	(e/d): 0.020–0.033 (p/e): 10–20 Re: 5000–50000	$St = \frac{f/2}{1+\sqrt{f/2}\{4.5(e^{+})^{0.28}Pr^{0.57}-0.95(P/e)^{0.55}\}}$	$f = \frac{(W+2B)f_s + W f_r}{2(W+B)}$ $fr = \frac{2}{[0.95(P/e)^{0.53}+2.5\ln(D/2e)-3.75]^2}$
Aharwal et al. [43]	Inclined rib with gap	(e/d): 0.0377 g/e: 0.5–2 d/W: 0.1667–0.667, W/H: 5.84 α: 60° Re: 3000–18000	$Nu = 0.002Re^{1.08(p/e)1.87} \times \exp[-0.45(\ln(p/e))^2](\alpha/60)^{0.006} \times \exp[-0.65(\ln \alpha/60)^2](d/W)^{-0.32} \times \exp[-0.12(\ln d/W)^2](g/e)^{-0.03} \times \exp[-0.18(\ln g/e)^2](e/D)^{0.5}$	$f = 0.071Re^{-0.133(p/e)1.83}\exp[-0.44(\ln(p/e))^2] \times (d/W)^{-0.43} \times \exp[-0.14(\ln d/W)^2](g/e)^{-0.052} \times (\alpha/60)^{0.67} (\exp[0.12(\ln g/e)^2](e/D)^{0.69}$
Muluwork and Saini [43]	V-shaped rib	(e/d): 0.01–0.05 P'/P: 0.2–0.8 S'/S: 1.1–2.3 B/S: 3–9 α: 30°–90° Re: 3032–17652	$Nu = 0.00534Re^{1.299}(B/S)^{1.346}(S'/S)^{1.112}(e/D)^{0.270}(P'/P)^{0.762} \exp[-2.25(\ln(P'/P))^2\exp[-0.376(\ln(1-\alpha/60))^2$	$f = 0.7117Re^{-0.299}(B/S)^{0.636}(S'/S)^{0.712}(e/D)^{0.113}(P'/P)^{-0.0936} \exp[-1.26(\ln(1-\alpha/70))^2$
Verma and Prasad [58]	Circular transverse wire	(e/d): 0.02–0.034 (p/e):10–40 Re: 5000–20,000	$Nu = 0.08596(p/e)^{-0.054}(e/D)^{0.072}Re^{0.723}$ for $e^{+} \le 24$ $Nu = 0.02954(p/e)^{-0.016}(e/D)^{0.021}Re^{0.802}$ for $e^{+} > 24$	$f = 0.245((p/e))^{-0.206}(e/D)^{0.243}Re^{-1.25}$
Gupta et al. [61]	Angled circular rib	(e/d): 0.020–0.05 (p/e): 7.5 and 10 α: 30°–90° Re: 3000–18,000	$Nu = 0.0024(e/D)^{0.001}(W/H)^{-0.06}Re^{1.084} \times \exp[-0.004(1-\alpha/60)^2]$ for $e^{+} < 35$ $Nu = 0.0071(e/D)^{-0.24}(W/H)^{-0.028}Re^{0.88} \times \exp[-0.475(1-\alpha/60)^2]$ for $e^{+} \ge 35$	$f = 0.1911(e/D)^{0.196}(W/H)^{-0.093}Re^{1.084} \times \exp[-0.993(1-\alpha/70)^2]$
Saini and Saini [62]	Wire mesh	(e/d): 0.012–0.039 S/e: 15.62–46.87 L/e: 25–71.87 Re: 1900–13,000	$Nu = 4.0 \times 10^{-4} \times Re^{1.22}(e/D)^{0.625}(S/e)^{2..22} \times \exp[-1.25\{\ln(S/10e)\}^2](L/e)^{2.26} \times \exp[-0.824(\ln(L/10e))^2]$	$f = 0.815Re^{0.361}(L/e)^{0.266}(S/10e)^{-0.19}(10(e/d))^{0.591}$
Momin et al. [63]	V-shaped ribs	(e/d): 0.01–0.03 (p/e): 10–40 Re: 2500–18,000	$Nu = 0.067Re^{0.888}(e/D)^{0.424}(\alpha/60)^{-0.077}\exp[-0.782(\ln \alpha/60)^2]$	$f = 6.266Re^{-0.425}(e/D)^{0.565}(\alpha/60)^{-0.093}\exp[-0.719 \times (\ln \alpha/60)^2]$
Karwa et al. [65]	Chamfered rib	W/H: 4.8, 6.1, 7.8, 9.66 and 12 (e/d): 0.0141–0.0328 (p/e): 4.5, 5.8, 7 and 8.5 Φ: −15, 0, 5, 10, 15 and 18 Re: 3000–20,000	$g = 103.77\, e^{-0.006\Phi}(W/H)^{0.5}(p/e)^{-2.56} \times \exp[0.7343\{\ln((p/e))\}^2](e^{+})^{-0.31}$ for $7 \le e^{+} < 20$ $g = 32.26(W/H)^{0.5}(p/e)^{-2.56} \times \exp[0.7343\{\ln((p/e))\}^2](e^{+})^{-0.08}$ for $20 \le e^{+} < 60$	$R = 1.66e^{-0.0078\Phi}(W/H)^{-0.4}(p/e)^{2.695} \times \exp[-0.762\{\ln((p/e))\}^2](e^{+})^{-0.075}$ for $5 \le e^{+} < 20$ $R = 1.325e^{-0.0078\Phi}(W/H)^{-0.4}(p/e)^{2.695} \times \exp[-0.762\{\ln((p/e))\}^2]$ for $20 \le e^{+} < 60$
Bhagoria et al. [66]	Wedge shaped rib	(e/d): 0.015–0.033 (p/e): 60.17 $\Phi^{-1.0264} < (p/e) < 12.15$ Re: 3000–18,000	$Nu = 1.89 \times 10^{-4}Re^{1.21}((e/d))^{0.426}((p/e))^{2.94} \times \exp[-0.71\{\ln((p/e))\}^2(\Phi/10)^{-0.018} \times \exp[-1.5\{\ln(\Phi/10)\}^2]$	$f = 12.44Re^{-0.18}((e/d))^{0.99}((p/e))^{-0.52}(\Phi/10)^{0.49}$
Saini and Saini [67]	Arc shaped rib	(p/e): 10 (e/d): 0.021–0.042	$Nu = 0.001047Re^{1.3186}(e/D)^{0.3772} \times (\alpha/90)^{-0.1198}$	$f = 0.14408Re^{-0.17103}(e/D)^{0.1765}(\alpha/90)^{0.1185}$

Table 3 (*Continued*)

Author	Roughness geometry	Parameters	Correlations	
			Heat transfer	Friction factor
Saini and Verma [68]	Dimple shape rib	Re: 2000–17,000 $\alpha/90$: 0.33–0.66 (e/d): 0.018–0.037 (p/e): 8–12	$Nu = 5.2 \times 10^{-4} Re^{1.27} \{(p/e)\}^{3.15} \times [\exp(-2.12)(\log((p/e)))^2](e/D)^{0.033} \times [\exp(-1.3)(\log((e/d))^2]$	$f = 0.642 Re^{-0.423} (p/e)^{-0.465} [\exp(0.054)(\log((p/e)))^2] \times (e/D)^{-0.0214} [\exp(0.84)(\log((e/d))^2]$
Karmare and Tikekar [69]	Metal grit rib	Re: 2000–12,000 (e/d): 0.035–0.044 (p/e): 12.5–36 l/s: 1.72–1	$Nu = 2.4 \times 10^{-3} \times Re^{1.3} \times (e/D)^{0.42} (l/s)^{-0.146} \times (p/e)^{-0.27}$	$f = 15.55 \times Re^{-0.263} \times (e/D)^{0.91} (l/s)^{-0.27} \times (p/e)^{-0.51}$
Jaurker et al. [71]	Rib-grooved	Re: 4000–17,000 (e/d): 0.022–0.040 (p/e): 4.5–10 g/P: 0.3–0.7	$Nu = 0.002062 Re^{0.936} ((e/d))^{0.349} (p/e)^{3.318} \times \exp[-0.868\{\ln(p/e)\}^2](g/P)^{1.108} \times \exp[2.486\{\ln(g/P)\}^2 + 1.406\{\ln(g/P)\}^3]$	$f = 0.001227 \times Re^{-0.199} ((e/d))^{0.585} (p/e)^{7.19} (g/P)^{0.645} \times \exp[-1.854\{\ln((p/e))\}^2] \times \exp[1.513\{\ln(g/P)\}^2 + 0.8662\{\ln(g/P)^3]$
Layek et al. [72]	Chamfered rib-grooved	Re: 3000–21,000 (e/d): 0.018–0.036 (p/e): 4.5–10 g/P: 0.3–0.7 Φ: 5–30	$Nu = 0.00225 Re^{0.92} ((e/d))^{0.52} (p/e)^{1.72} \times \exp[-0.22(\ln \Phi)^2] \times \exp[-0.46\{\ln (p/e)\}^2](g/P)^{-1.21} \Phi^{1.24} \times \exp[-0.74\{\ln(g/P)\}^2]$	$f = 0.00245 \times Re^{-0.124} ((e/d))^{0.365} (p/e)^{4.32} (g/P)^{-1.124} \times \exp[-1.09\{\ln((p/e))\}^2] \times \exp[-0.68\{\ln(g/P)\}^2] \times \exp[0.005\Phi]$
Varun et al. [73]	Inclined and transverse rib	Re: 3000–21,000 (e/d): 0.030 (p/e): 3–8 Re: 2000–14,000	$Nu = 0.0006 Re^{1.213} (p/e)^{0.0104}$	$f = 1.0858 Re^{-0.3685} (p/e)^{0.0114}$

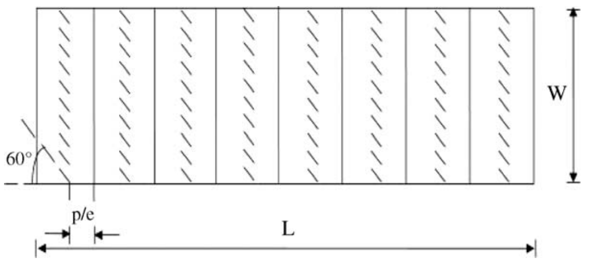


Fig. 27. Combination of transverse and inclined roughness [73].

value of 10, relative groove position (g/P) value of 0.4 provided about 2.42 and 2.6 times increase in the Nusselt number and friction factor respectively for entire range of Reynolds number (Re) studied. Correlations for Nusselt number and friction factor were developed. The geometry investigated has been shown in Fig. 26.

5.12.3. Combination of inclined and transverse ribs

Varun et al. [73] carried out an experimental study on heat transfer and friction characteristics by using a combination of inclined and transverse ribs on the absorber plate of a solar air heater with Reynolds number (Re) ranging from 2000 to 14,000, relative roughness pitch (p/e) range of 3–8, relative roughness height (e/D) value of 0.030, duct aspect ratio (W/H) value of 10 and roughness height (e) value of 1.6 mm. For relative roughness pitch (p/e) value of 8, the best thermal performance was reported. Correlations for Nusselt number and friction factor were developed. The geometry investigated has been shown in Fig. 27.

5.13. Computational analysis

Chaube et al [74] carried out a computational analysis using Fluent 6.1 software to investigate the flow and heat transfer characteristics of two-dimensional rib roughened rectangular ducts with one wall subjected to uniform heat flux of 1100 W/m^2. They compared the predictions of different turbulence models with experimental results available in the literature and reported good matching of experimental results and predictions of shear stress transport (SST) K-ω turbulence model. They used SST K-ω turbulence model for analysing the performance of nine different roughness elements and compared the predictions on the basis of heat transfer enhancement, friction characteristics and performance index. The results obtained from two-dimensional model were reported to be closer to the experimental results and these models required less memory and computational time as compared to three-dimensional models. The highest heat transfer was reported in case of chamfered ribs, however, the best performance index was found to be with rectangular rib of size 3 mm × 5 mm with in the range of parameters investigated.

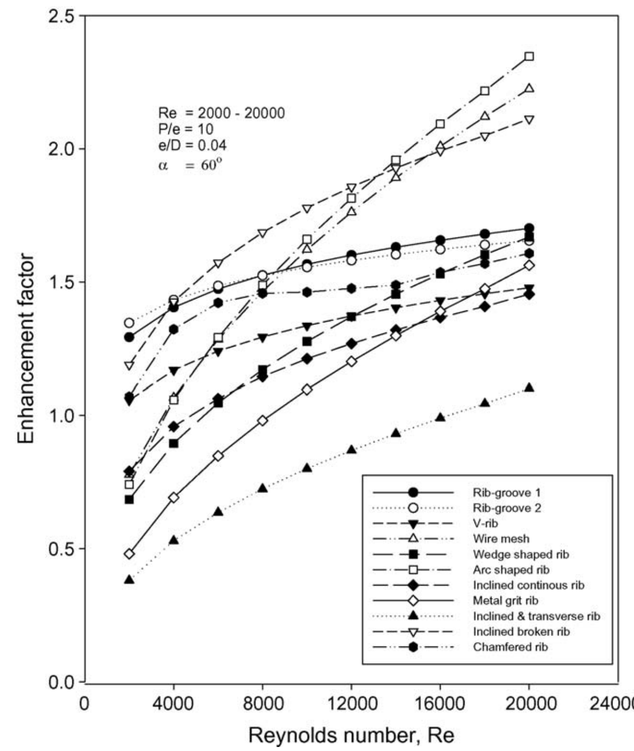


Fig. 28. Comparison of enhancement factor of different geometries.

Sharad [75] analysed the effects of arc shaped roughness geometry on heat transfer and friction by computational fluid dynamics (CFD). The results obtained from different models of computational analysis were compared with Dittus–Boelter empirical relationship for smooth duct and it was found that the Renormalization (RNG) k-ε model had least variation as compared to other CFD models.

6. Comparison of thermohydraulic performance of roughened solar air heaters

Thermal performance of solar air heaters improves with the inclusion of roughness geometry in the form of repeated ribs on absorber plates, which also results in higher friction factor and consequently increases the pumping power requirements. In order to determine the geometry of artificial roughness elements that maximizes the convective heat transfer coefficient with minimum pumping power requirements, thermohydraulic performance has been compared using the correlations of heat transfer and friction factor for different roughness geometries given in Table 3. Wright et al. [52] defined a parameter called enhancement factor ($\acute{e}$) in

Table 4
Roughness geometries and parameters.

S. no.	Roughness geometry	Parameters
1.	Inclined broken ribs [43]	$(p/e) = 10$, $(e/d) = 0.04$, Re = 2000–20,000, $W/H = 11.5$, $\alpha = 60^\circ$, $g/e = 1$, $d/W = 0.25$
2.	Inclined continuous rib [61]	$(p/e) = 10$, $(e/d) = 0.04$, Re = 2000–20,000, $W/H = 11.5$, $\alpha = 60^\circ$
3.	Wire mesh [62]	$(p/e) = 10$, $(e/d) = 0.04$, Re = 2000–20,000, $S/e = 25$, $L/e = 46.87$
4.	V-rib [63]	$(p/e) = 10$, $(e/d) = 0.04$, Re = 2000–20,000, $\alpha = 60^\circ$
5.	Chamfered rib [65]	$(p/e) = 10$, $(e/d) = 0.04$, Re = 2000–20,000, $\varphi = 15^\circ$
6.	Wedge shaped rib [66]	$(p/e) = 10$, $(e/d) = 0.04$, Re = 2000–20,000, $\varphi = 10^\circ$
7.	Arc shaped rib [67]	$(p/e) = 10$, $(e/d) = 0.04$, Re = 2000–20,000, $\alpha = 30^\circ$
8.	Metal grit rib [69]	$(p/e) = 10$, $(e/d) = 0.04$, Re = 2000–20,000, $l/s = 1.72$
9.	Rib-groove 1 [71]	$(p/e) = 10$, $(e/d) = 0.04$, Re = 2000–20,000, $g/P = 0.4$
10.	Rib-groove 2 [72]	$(p/e) = 10$, $(e/d) = 0.04$, Re = 2000–20,000, $\varphi = 18^\circ$, $g/P = 0.4$
11.	Inclined-transverse ribs [73]	$(p/e) = 10$, $(e/d) = 0.04$, Re = 2000–20,000

terms of Nusselt number ratio and friction factor ratio of roughened and smooth channels which is expressed as

$$\hat{\varepsilon} = \frac{(\mathrm{Nu}/\mathrm{Nu_s})}{(f/f_s)^{0.33}} \tag{11}$$

Thermohydraulic comparison of different roughness geometries has been shown in Fig. 28. The roughness element geometries and the parameters considered for the comparison have been given in Table 4. Fig. 28 shows the variation of enhancement factor with Reynolds number (Re) for different roughness geometries used in solar air heaters. Amongst all the roughness geometries considered, inclined broken rib geometry has the best thermohydraulic performance followed by arc shaped rib, wire mesh and rib-groove one geometries for the Reynolds number range between 3000 and 14,000. For Reynolds number range beyond 14,000, arc shaped geometry followed by wire mesh geometry outperforms the other roughness geometries. Thermohydraulic performance of combination geometries such as rib-groove 1 and 2 is almost same with rib-groove 2 arrangement outperforming the rib-groove 1 arrangement in the lower range of Reynolds number up to 6000 and in the higher range of Reynolds number, rib-groove 1 arrangement performed better for the range of parameters considered.

7. Discussions

Based on the literature survey conducted extensively on thermohydraulic performance of artificially roughened solar air heaters, it has been found that roughness, on the absorber plate of a solar air heater, is produced mostly by fixing wires [7,8,10,11,18–22], machining as in case of rib-groove geometry [35,36] or welding ribs. However, it has been observed that process of producing artificial roughness by these methods may be a tedious proposition. However, use of artificial roughness results in size reduction of solar air heaters if heat exchange rate is kept constant or if size is kept constant it aids in increasing heat extraction by air from the absorber plate, thereby, maximizing the heat transfer.

For better understanding of heat transfer enhancement and flow processes due to turbulence generated by the presence of roughness on absorber plate of a solar air heater, theoretical and numerical studies need to be carried out. A few studies, based on computational fluid dynamics (CFD), have been carried out by Chaube et al. [74] and Sharad [75] using Fluent 6.1 software. However, efforts are required to develop models that depict the turbulence and secondary flow, which play significant role in heat transfer enhancement in roughened solar air heaters. In the absence of accurate and reliable model, flow visualisation techniques should be used to overcome the difficulties faced to describe the heat transfer and flow characteristics mathematically. It has been found that only Ahrwal et al. [43] used Particle Image Velocimetry (PIV) system for flow visualisation.

Most of the experimental investigations carried out for performance improvement of solar air heaters involve single surface enhancement techniques such as transverse, inclined, v-shape, w-shape ribs, etc. Though simultaneous use of two or more enhancement techniques produces better results in comparison to individual technique [34], few studies [71–73] involving use of compound enhancement techniques in solar air heater have been reported in literature. Compound heat transfer enhancement techniques offer a way to further improve thermal performance of a solar air heater and this area of enhancement technology holds much promise for future developments.

Invariably, use of roughness geometry in a solar air heater substantially improves its thermal performance but at the cost of considerable drop in pressure of flowing fluid, which affects thermohydraulic performance adversely. Therefore, geometry and orientation of roughness elements should be chosen in such a way that enhancement in heat transfer is accompanied by acceleration of flow or pressure drop is minimum as in case of inclined ribs with gap [42] and arc shaped ribs [67] respectively.

8. Conclusions

In the present study, a review of roughness element geometries has been carried out and thermohydraulic performance of solar air heaters roughened with these roughness element geometries has been compared in order to determine the best performing roughness geometry. From the review, following conclusions are drawn:

1. Use of artificial roughness brings about a substantial improvement in the performance of the solar air heater resulting in size reduction or maximization of heat transfer rate. Thereby, conserving energy along with savings in material cost.
2. Experimental investigations employing compound enhancement techniques could be more useful in order to achieve greater improvement in thermal performance of solar sir heaters.
3. Using computational fluid dynamics (CFD) models, analysis of heat transfer and flow characteristics of roughened solar air heaters needs to be carried out to predict optimum roughness element parameters.
4. In artificially roughened solar air heaters, there is lot of scope for use of flow visualisation techniques in order to analyse flow and heat transfer enhancement processes.
5. Thermohydraulic performance of inclined broken rib geometry has been found to be better in comparison to other roughness element geometries for Reynolds number range between 3000 and 14,000 and beyond which arc shaped geometry outperforms the inclined broken rib geometry with in the range of roughness parameters considered.

References

[1] Manglik R. In: Benjan A, Kraus AD, editors. Heat transfer handbook. New Jersey: John Wiley & Sons; 2003 [chapter four].
[2] Constantinos AB. A review of augmentation techniques for heat transfers surfaces in single-phase heat exchangers. Energy 1990;15:899–906.
[3] Han JC. Heat transfer and friction characteristics in rectangular channels with rib turbulators. ASME J Heat Transfer 1988;131:321–8.
[4] Han JC, Glicksman LR, Rohsenow WM. An investigation of heat transfer and friction for rib-roughened surfaces. Int J Heat Mass Transfer 1978;121:1143–56.
[5] Han JC, Park JS, Lei CK. Heat transfer enhancement in channels with turbulence promoters. ASME J Gas Turbines Power 1985;107:628–35.
[6] Webb RL, Eckert RG, Goldstein RJ. Heat transfer and friction in tubes with repeated-rib roughness. Int J Heat Mass Transfer 1971;26:601–17.
[7] Donnet MD, Meyer L. Turbulent convective heat transfer from rough surfaces with two-dimensional rectangular ribs. Int J Heat Mass Transfer 1977;20:583–620.
[8] Olsson CO, Sunden B. Experimental study of flow and heat transfer in rib-roughened rectangular channels. Exp Thermal Fluid Sci 1998;16:349–65.
[9] Han JC, Zhang YM, Lee CP. Augmented heat transfer in square channels with parallel, crossed and V-shaped angled ribs. ASME J Heat Transfer 1991;1:37–52.
[10] Taslim ME, Li T, Kercher DM. Experimental heat transfer and friction in channels roughened with angled, v-shaped and discrete ribs on two opposite walls. ASME J Turbomach 1996;118:20–8.
[11] Liou TM, Chen CC, Tsai TW. Heat transfer and fluid flow in a square duct with 12 different shaped vortex generators. ASME J Heat Transfer 2000;122:327–35.
[12] Chandra PR, Alexander CR, Han JC. Heat transfer and friction behaviors in rectangular channels with varying number of ribbed walls. Int J Heat Mass Transfer 2003;40:481–95.
[13] Bilen K, Akyo U, Yapici S. Heat transfer and friction correlations and thermal performance analysis for a finned surface. Energy Conversion Manage 2001;42:1071–83.
[14] Yeh RY. An analytical study of the optimum dimensions of rectangular fins and cylindrical pin-fins. Int J Heat Mass Transfer 1997;40:3607–15.
[15] Voanfossen GJ. Heat transfer coefficients for staggered arrays of short pin fins. Trans ASME J Heat Transfer 1982;104:268–74.
[16] Sparrow EM, Charmchi M. Heat transfer and fluid flow characteristics of span wise-periodic corrugated ducts. Int J Heat Mass Transfer 1980;23:471–81.

[17] Sherony DF, Solbrig CW. Analytical investigation of heat or mass transfer and friction factors in a corrugated duct of heat or mass exchanger. Int J Heat Mass Transfer 1970;13:145–6.
[18] Asako Y, Nakamura H, Faghri M. Heat transfer and pressure drop characteristics in a corrugated duct with rounded corners. Int J Heat Mass Transfer 1988;31:1237–45.
[19] Islamoglu Y, Parmaksizoglu C. Numerical investigation of convective heat transfer and pressure drop in a corrugated heat exchanger channel. Appl Thermal Eng 2004;24:141–7.
[20] Hwang SD, Jang IH, Cho HH. Experimental study on flow and local heat/mass transfer characteristics inside corrugated duct. Int J Heat Fluid Flow 2006;27:21–32.
[21] Buchlin JM. Convective heat transfer in a channel with perforated ribs. Int J Thermal Sci 2002;41:332–40.
[22] Liou TM, Chen SH. Turbulent heat and fluid flow in passage distributed by detached perforated ribs of different heights. Int J Heat Mass Transfer 1998;41:1795–6.
[23] Saraç BA, Bali T. An experimental study on heat transfer and pressure drop characteristics of decaying swirl flow through a circular pipe with a vortex generator. Exp Thermal Fluid Sci 2007;32:158–65.
[24] Promvonge P, Eiamsa-ard S. Heat transfer behaviors in a tube combined with conical-ring and twisted tape insert. Int Commun Heat Mass Transfer 2007;34:849–59.
[25] Saha SK, Dutta A, Dahl SK. Friction and heat transfer characteristics of laminar flow through a circular tube fitted with regularly spaced twisted-tape elements. Int J Heat Mass Transfer 2001;44:4211–23.
[26] Marner WJ, Bergles AE. Augmentation of highly viscous laminar tube side heat transfer by means of a twisted-tape insert and an internally finned tube. ASME HTD 1985;43:19–28.
[27] Nakamura M, Suguwara M, Kozuka M. Heat transfer characteristics in a two-dimensional channel with an oscillating wall. Heat-Transfer Asian Res 2001;30:280–92.
[28] Dutta S, Andrews MJ, Han JC. Prediction of turbulent heat transfer in rotating smooth square ducts. Int J Heat Mass Transfer 1996;39:2505–14.
[29] Murata A, Mochizuki S, Takahashi T. Local heat transfer measurements of an orthogonally rotating square duct with angled rib turbulators. Int J Heat Mass Transfer 1999;42:3047–56.
[30] Murata A, Mochizuk S. Effect of centrifugal buoyancy on turbulent heat transfer in an orthogonally rotating square duct with transverse or angled rib turbulators. Int J Heat Mass Transfer 2001;123:858–67.
[31] Aguilar G, Gasljevic K, Mattys EF. Asymptotes of maximum friction and heat transfer reduction for drag-reducing surfactant solutions. Int J Heat Mass Transfer 2001;44:2835–43.
[32] Kenning DBR, Kao YS. Convective heat transfer to water containing bubbles: enhancement not dependent on thermocapillarity. Int J Heat Mass Transfer 1970;15:1709–17.
[33] Fujii M, Seshimo Y, Yamanaka G. Heat transfer and pressure drop of perforated heat exchanger with passage enlargement and contraction. Int J Heat Mass Transfer 1988;31:135–42.
[34] Lin YL, Shih TIP, Stephen MA, Chyu MK. A numerical study of flow and heat transfer in a smooth and ribbed u-duct with and without rotation. ASME J Heat Transfer 2001;123:219–32.
[35] Varun, Saini RP, Singal SK. A review on roughness geometry used in solar air heaters. Solar Energy 2007;81:1340–50.
[36] Mittal MK, Varun, Saini RP, Singal SK. Effective efficiency of solar air heaters having different types of roughness elements on absorber plate. Energy 2007;32:739–45.
[37] Bhatti MS, Shah RK. Turbulent and transition flow convective heat transfer in ducts. In: Kakac S, Shah RK, Aung W, editors. Hand book of single-phase convective heat transfer. New York: John Willey & Sons; 1987 [chapter 4].
[38] Nikuradse J. Laws of flow in rough pipes. NACA Technical Memorandum 1958;1292.
[39] Dippery DF, Sabersky RH. Heat and momentum transfer in smooth and rough tubes at various Prandtl numbers. Int J Heat Mass Transfer 1963;36:1459–69.
[40] Prasad BN, Saini JS. Optimal thermohydraulic performance of artificially roughened solar air heaters. Solar Energy 1991;47:91–6.
[41] Prasad BN, Saini JS. Effect of artificial roughness on heat transfer and friction factor in a solar air heater. Solar Energy 1988;41:555–60.
[42] Taslim ME, Li T, Kretcher DM. Experimental heat transfer and friction in channels roughened with angled, v-shaped and discrete ribs on two opposite walls. Trans ASME J Turbomachinery 1996;118:20–8.
[43] Aharwal KR, Gandhi BK, Saini JS. Experimental investigation on heat-transfer enhancement due to a gap in an inclined continuous rib arrangement in a rectangular duct of solar air heater. Renew Energy 2008;33:585–96.
[44] Muluwork KB. Investigations on fluid flow and heat transfer in roughened absorber solar heaters. Ph.D. Dissertation 2000; IIT, Roorkee-247667, India.
[45] Sparrow EM, Hossfeld LM. Effect of rounding of protruding edges on heat transfer and pressure drop in a duct. Int J Heat Mass Transfer 1984;27: 1715–23.
[46] Lewis MJ. Optimizing the thermohydraulic performance of rough surfaces. Int J Heat Mass Transfer 1975;18:1243–8.
[47] Altfeld K, Leiner W, Fiebg M. Second Law optimization of flat plate solar air heaters. Solar Energy 1988;41:309–17.
[48] Cortes A, Piacentini R. Improvement of efficiency of a bare solar collector by means of turbulence promoters. Appl Energy 1990;36:253–61.
[49] Joule JP. On the surface condensation of steam. Philos Trans R Soc Lond 1861;151:133–60.
[50] Bergles AE. New frontiers in enhanced heat transfer. In: Manglik RM, editor. Advances in enhanced heat transfer. New York: ASME; 2000. p. 1–8.
[51] Bergles AE. ExHFT for fourth generation heat transfer technology. Exp Thermal Fluid Sci 2002;26:335–44.
[52] Wright LM, Fu WL, Han JC. Thermal performance of angled, V-shaped and W-shaped rib turbulators in rotating rectangular cooling channels (AR = 4:1). Trans ASME 2004;126:604–14.
[53] Han JC, Zhang YM, Lee CP. Augmented heat transfer in square channels with parallel, crossed and v-shaped angled ribs. Trans ASME J Heat Transfer 1991;113:590–6.
[54] Han JC, Zhang YM. High performance heat transfer ducts with parallel, broken and v-shaped broken ribs. Int J Heat Mass Transfer 1992;35:513–23.
[55] Kays WM, London AL. Compact heat exchangers. New York: McGraw Hill; 1966.
[56] Prasad K, Mullick SC. Heat transfer characteristics of a solar air heater used for drying purposes. Appl Energy 1983;13:83–93.
[57] Gupta D, Solanki SC, Saini JS. Heat and fluid flow in rectangular solar air heater ducts having transverse rib roughness on absorber plates. Solar Energy 1993;51:31–7.
[58] Verma SK, Prasad BN. Investigation for the optimal thermohydraulic performance of artificially roughened solar air heaters. Renew Energy 2000;20:19–36.
[59] Karwa RK. Experimental studies of augmented heat transfer and friction in asymmetrically heated rectangular ducts with ribs on heated wall in transverse, inclined, v-continuous and v-discrete pattern. Int Commun Heat Mass Transfer 2003;30:241–50.
[60] Sahu MM, Bhagoria JL. Augmentation of heat transfer coefficient by using 90° broken transverse ribs on absorber plate of solar air heater. Renew Energy 2005;30:2057–63.
[61] Gupta D, Solanki SC, Saini JS. Thermohydraulic performance of solar air heaters with roughened absorber plates. Solar Energy 1997;61:33–42.
[62] Saini RP, Saini JS. Heat transfer and friction factor correlations for artificially roughened ducts with expanded metal mesh as roughened element. Int J Heat Mass Transfer 1997;40:973–86.
[63] Momin AME, Saini JS, Solanki SC. Heat transfer and friction in solar air heater duct with v-shaped rib roughness on absorber plate. Int J Heat Mass Transfer 2002;45:3383–96.
[64] Karwa R, Bairwa RD, Jain BP, Karwa N. Experimental study of the effects of rib angle and discretization on heat transfer and friction in an asymmetrically heated rectangular duct. J Enhanced Heat Transfer 2005;12:343–55.
[65] Karwa R, Solanki SC, Saini JS. Heat transfer coefficient and friction factor correlations for the transitional flow regime in rib-roughened rectangular ducts. Int J Heat Mass Transfer 1999;42:1597–615.
[66] Bhagoria JL, Saini JS, Solanki SC. Heat transfer coefficient and friction factor correlations for rectangular solar air heater duct having transverse wedge shaped rib roughness on the absorber plate. Renew Energy 2002;25:341–69.
[67] Saini SK, Saini RP. Development of correlations for Nusselt number and friction factor for solar air heater with roughened duct having arc-shaped wire as artificial roughness. Solar Energy 2008;82:1118–30.
[68] Saini RP, Verma J. Heat transfer and friction factor correlations for a duct having dimple-shaped artificial roughness for solar air heaters. Energy 2008;l33:1277–87.
[69] Karmare SV, Tikekar AN. Heat transfer and friction factor correlation for artificially roughened duct with metal grit ribs. Int J Heat Mass Transfer 2007;50:4342–51.
[70] Kumar A, Bhagoria JL, Sarviya RM.In: 19th National & 8th ISHMT-ASME Heat and Mass Transfer Conference; Heat transfer enhancement in channel of solar air collector by using discrete w-shaped artificial roughened absorber 2008.
[71] Jaurker AR, Saini JS, Gandhi BK. Heat transfer and friction characteristics of rectangular solar air heater duct using rib-grooved artificial roughness. Solar Energy 2006;80:895–7.
[72] Layek A, Saini JS, Solanki SC. Second law optimization of a solar air heater having chamfered rib-groove roughness on absorber plate. Renew Energy 2007;32:1967–80.
[73] Varun, Saini RP, Singal SK. Investigation of thermal performance of solar air heater having roughness elements as a combination of inclined and transverse ribs on absorber plate. Renew Energy 2008;l33:1398–405.
[74] Chaube A, Sahoo PK, Solanki SC. Analysis of heat transfer augmentation and flow characteristics of a solar air heater. Renew Energy 2006;31:317–31.
[75] Kumar S. CFD based heat transfer analysis of artificially roughened solar air heater. M. Tech Dissertation 2008, Departmental Library AHEC, IIT Roorkee-247667.